

# Magnetism of the $s = 1/2$ $J_1$ - $J_2$ square-kagome lattice antiferromagnet

Johannes Richter<sup>1,2,\*</sup> and Jürgen Schnack<sup>3,†</sup>

<sup>1</sup>*Institut für Physik, Universität Magdeburg, P.O. Box 4120, D-39016 Magdeburg, Germany*

<sup>2</sup>*Max-Planck-Institut für Physik Komplexer Systeme,  
Nöthnitzer Straße 38, D-01187 Dresden, Germany*

<sup>3</sup>*Fakultät für Physik, Universität Bielefeld, Postfach 100131, D-33501 Bielefeld, Germany*

(Dated: June 22, 2023)

Over the last decade, the spin-1/2 Heisenberg antiferromagnet on the square-kagome (SK) lattice has attracted growing attention as a model system of highly frustrated quantum magnetism. A further motivation for theoretical studies of this model comes from the recent discovery of SK spin-liquid compounds  $\text{KCu}_6\text{AlBiO}_4(\text{SO}_4)_5\text{Cl}$  [M. Fujihala et al., *Nat. Commun.* **11**, 3429 (2020)] and  $\text{Na}_6\text{Cu}_7\text{BiO}_4(\text{PO}_4)_4[\text{Cl}(\text{OH})]_3$  [O. V. Yakubovich et al. *Inorg. Chem.* **60**, 11450 (2021)]. The SK antiferromagnet exhibits two non-equivalent nearest-neighbor bonds  $J_1$  and  $J_2$ . One may expect that in SK compounds  $J_1$  and  $J_2$  are of different strength. Here, we present a numerical study of finite systems of  $N = 30$ ,  $36$  and  $N = 42$  sites by means of the finite-temperature Lanczos method. We discuss the temperature dependence of the Wilson ratio  $P(T)$ , the specific heat  $C(T)$ , the entropy  $S(T)$ , and of the susceptibility  $X(T)$  of the  $J_1$ - $J_2$  SK Heisenberg antiferromagnet varying  $J_2/J_1$  in a range  $0 \leq J_2/J_1 \leq 4$ . We also discuss the zero-field ground state of the model. We find indications for a magnetically disordered singlet ground state for  $0 \leq J_2/J_1 \lesssim 1.65$ . Beyond  $J_2/J_1 \sim 1.65$  the singlet ground state gives way for a ferrimagnetic ground state which becomes a stable Lieb ferrimagnet with magnetization  $M = N/6$  (UUD state) for  $J_2/J_1 \gtrsim 1.83$ . In the region  $0.77 \lesssim J_2/J_1 \lesssim 1.65$  the low-temperature thermodynamics is dominated by a finite singlet-triplet gap filled with low-lying singlet excitations leading to an exponentially activated low-temperature behavior of  $X(T)$ . On the other hand, the low-lying singlets yield an extra maximum or a shoulder-like profile below the main maximum in the  $C(T)$  curve. For  $J_2/J_1 \lesssim 0.7$  the low-temperature thermodynamics is characterized by a large fraction of  $N/3$  weakly coupled spins leading to a sizable amount of entropy at very low temperatures. In an applied magnetic field the magnetization process features plateaus and jumps in a wide range of  $J_2/J_1$ .

PACS numbers: 75.10.Jm, 75.50.Xx, 75.40.Mg

## I. INTRODUCTION

Highly frustrated quantum antiferromagnets on two-dimensional lattices have attracted an enormous attention over more than three decades, see, e.g., [1–5]. "Now in the early 2020s, quantum magnetism is a mature field showing no signs of senescence. To the contrary, there is a tremendous amount of activity studying exotic magnetic phenomena especially with strong quantum fluctuations." [6] Over many years the kagome antiferromagnet (KHAF) has been the holy grail in this field. Quite recently the square-kagome antiferromagnet, the 'little brother' of the kagome antiferromagnet, has received more appreciation because several magnetic compounds with square-kagome lattice structure have been found which do not exhibit magnetic order down to very low temperatures [7–10]. The square-kagome lattice (sometimes also called shuriken or squagome lattice) [11–14] is a two-dimensional tiling built of squares and corner-sharing triangles. The classical ground state of the square-kagome Heisenberg antiferromagnet (SKHAF) is highly degenerated (classical spin liquid). There are

two non-equivalent sites A and B as well as two non-equivalent nearest-neighbor bonds  $J_1$  and  $J_2$ , see the left inset in Fig. 1. The theoretical study of the quantum model started 20 years ago [11–13, 15–17]. Already at that time evidence for the absence of ground-state magnetic order was found [12, 13].

Starting in 2013 the interest in the spin-1/2 SKHAF has been growing as a model system exhibiting a non-magnetic quantum ground state, magnetization plateaus, flat-band physics near the saturation field and quantum scars [14, 17–29]. All these papers were focused on zero-temperature properties. Only, in the early paper [16] specific-heat data calculated by a simple renormalization group approach were reported. The thermodynamics of the balanced spin-1/2 SKHAF, i.e.,  $J_1 = J_2 = J$ , has been studied quite recently in Ref. [30] using the finite-temperature Lanczos method (FTLM). At zero magnetic field we find that the KHAF and SKHAF exhibit a striking similarity of the temperature profile of  $C(T)$ ,  $X(T)$  and  $S(T)$  down to very low temperature  $T$ . Thus, for  $X(T)$  and  $S(T)$  an almost perfect coincidence for both models was observed. For the specific heat there is a perfect agreement of the  $C(T)$  data down to  $T/J = 0.3$ . A characteristic feature common in both models is the existence of low-energy singlet excitations filling the magnetic spin gap [13, 31–33]. These low-energy singlets yield a low-temperature shoulder below

\* Johannes.Richter@physik.uni-magdeburg.de

† jschnack@uni-bielefeld.de

the major maximum in the  $C(T)$  profile [30, 34]. We mention that such a shoulder has been observed in a recent experiment on the kagome quantum antiferromagnet  $\text{YCu}_3(\text{OH})_6\text{Br}_2[\text{Br}_x(\text{OH})_{1-x}]$  [35]. The subtle details of the singlet excitations depending on the shape and the size  $N$  of the finite lattices lead to deviations between the behavior of  $C(T)$  for both models at very low  $T$ .

Bearing in mind the recent experimental studies on square-kagome quantum antiferromagnets [7–10] and the non-equivalence of the nearest-neighbor bonds  $J_1$  and  $J_2$  we may expect that for the modeling of square-kagome compounds it is natural to consider a spin model with  $J_1 \neq J_2$ . Moreover, the  $J_1$ - $J_2$  model is interesting in its own right as highly frustrated model that allows to tune the competition between the bonds.

So far only a few papers exist which study the zero-temperature properties of the  $J_1$ - $J_2$  model [18, 20, 23–25] where in Ref. [23] the focus is on the magnetization process of the  $J_1$ - $J_2$  model with only slight deviations from the balanced model, i.e., the difference between  $J_1$  and  $J_2$  is small. In our paper we will fill the gap of missing nonzero-temperature studies and present FTLM data for the magnetization  $M$ , the Wilson ratio  $P$ , the specific heat  $C$ , the entropy  $S$  and the uniform magnetic susceptibility  $X$  of the  $J_1$ - $J_2$  SKHAF. In addition, we will analyze the ground state of the finite lattices used for the FTLM studies which allows to get a relation between ground-state and finite-temperature properties of the investigated systems.

The corresponding Heisenberg Hamiltonian augmented with a Zeeman term is given by

$$H = J_1 \sum_{\langle i,j \rangle_1} \mathbf{s}_i \cdot \mathbf{s}_j + J_2 \sum_{\langle i,j \rangle_2} \mathbf{s}_i \cdot \mathbf{s}_j + g\mu_B B \sum_i s_i^z, \quad (1)$$

where  $s_i^2 = s(s+1) = 3/4$ . The  $J_1$  bonds represent the nearest-neighbor exchange connecting A sites on the squares, whereas the  $J_2$  bonds represent the nearest-neighbor exchange connecting A with B sites on the triangles, see the left inset in Fig. 1. In what follows we set  $J_1 = 1$ .

The paper is organized as follow. In Section II we introduce our numerical scheme. In Section III we present our results where in Section III A we briefly discuss the ground-state properties as well as the excitation gaps of the model which may be relevant for the interpretation of the low-temperature thermodynamics. The results for the temperature dependence of the Wilson ratio  $P(T)$ , the specific heat  $C(T)$ , the entropy  $S(T)$  as well as the susceptibility  $X(T)$  at zero magnetic field are presented and discussed in Section III B. Finally, in Section III C we discuss the magnetization process in an applied magnetic field. In the last Section IV we summarize our findings. In two appendices we show the finite lattices considered in our paper (App. A) and provide some additional figures to illustrate finite-size effects (App. B).

## II. CALCULATION SCHEME

The magnetic system under consideration is modeled by the spin-1/2 Heisenberg Hamiltonian given in Eq. (1). We use the conservation of the  $z$ -component of the total spin  $S^z = \sum_i s_i^z$  as well as lattice symmetries, i.e., the Hilbert space splits into subspaces characterized by the eigenvalues of  $S^z$  (magnetic quantum number  $M$ ) and of the symmetry operator, see, e.g., Refs. [36, 37]. To calculate the ground state we perform Lanczos exact diagonalization in the sector  $M = 0$ . For that we use Jörg Schulenburg’s publicly available package *spinpack* [38, 39].

For the FTLM scheme we also exploit the package *spinpack* as well as the conservation of  $S_z$  and the symmetries to decompose the Hilbert space into much smaller subspaces. The FTLM is meanwhile a well established and accurate approach to calculate thermodynamic quantities of frustrated quantum spin systems [30, 34, 40–55]. We do not present a detailed description of the method, rather we will provide the basics of the FTLM for convenience. Within the FTLM the sum over an orthonormal basis in the partition function is replaced by a much smaller sum over  $R$  random vectors:

$$Z(T, B) \approx \sum_{\gamma=1}^{\Gamma} \frac{\dim(\mathcal{H}(\gamma))}{R} \sum_{\nu=1}^R \sum_{n=1}^{N_L} e^{-\beta \epsilon_n^{(\nu)}} |\langle n(\nu) | \nu \rangle|^2, \quad (2)$$

where the  $|\nu\rangle$  label random vectors for each symmetry-related orthogonal subspace  $\mathcal{H}(\gamma)$  of the Hilbert space with  $\gamma$  labeling the respective symmetry. In Eq. (2), the exponential of the Hamiltonian has been replaced by its spectral representation in a Krylov space spanned by the  $N_L$  Lanczos vectors starting from the respective random vector  $|\nu\rangle$ , where  $|n(\nu)\rangle$  is the  $n$ -th eigenvector of  $H$  in this Krylov space.

For more information we refer the interested reader to the reviews [45, 48] and to our recent FTLM papers of the KHAF [34] and SKHAF [30]. A detailed discussion of the accuracy of the FTLM can be found in Refs. [34] and [53]. Based on this knowledge, we chose the number of random vectors  $R$  along the lines of our previous study [34].

## III. THE SKHAF AT ZERO MAGNETIC FIELD

### A. Analysis of the ground state of SKHAF on finite lattices of $N = 30$ and $N = 36$ sites

The absence of magnetic long-range order for the balanced  $s = 1/2$  SKHAF ( $J_1 = J_2$ ) was established by previous studies [13, 18, 20, 25, 28, 29]. The nature of the ground state is still under debate, candidates are a pinwheel valence-bond-crystal ground state [18, 28], a loop-six valence-bond state [20, 29] or a topological nematic spin liquid [25]. The ground-state phase diagram of the

$J_1$ - $J_2$  model was studied in Ref. [25] using a Schwinger-boson mean field theory as well as in Refs. [18, 20] using a resonating valence-bond approach.

Here we present Lanczos exact diagonalization data for  $N = 30$  and  $N = 36$ . Note that a brief discussion of the ground state for  $N = 24$  and  $N = 30$  was already given in Refs. [20, 24]. Our ground-state data will be useful to compare with the Schwinger-boson data [25] as well as for the interpretation of the low-temperature thermodynamics.

To get an impression on possible ground state magnetic order we first consider an order parameter introduced in Ref. [2] that measures the total strength of the overall spin-spin correlations without any assumptions on possible magnetic order with a related ordering vector  $\mathbf{Q}$ . It is defined as

$$m^+ = \frac{1}{N^2} \sum_{i,j}^N |\langle \mathbf{s}_i \cdot \mathbf{s}_j \rangle|. \quad (3)$$

Numerical ground-state data for  $m^+$  are depicted in Fig. 1, main panel. It is obvious that in a wide parameter range  $0 \leq J_2 \lesssim 1.65$  the order parameter  $m^+$  is approximately of the same small size as for the balanced model ( $J_2 = 1$ ) which is known to be in a non-magnetic singlet ground state. The steep increase of  $m^+$  beyond  $J_2 \approx 1.65$  is related to a transition from a singlet ground state to a ferrimagnetic ground state with non-zero magnetization  $M$ . The jumps in the  $m^+(J_2)$  curve visible for  $1.65 \lesssim J_2 \lesssim 1.83$  are related to a stepwise increase of  $M$  up to  $M_{1/3} = M_{\text{sat}}/3$ . The ground state with  $M_{1/3}$  present for  $J_2 \gtrsim 1.83$  is a ferrimagnetic up-up-down (UUD) state, i.e.,  $\langle s_{i \in A}^z \rangle$  and  $\langle s_{i \in B}^z \rangle$  are antiparallel. To give an example, for  $N = 36$ ,  $J_2 = 2$ , we have  $\langle s_{i \in A}^z \rangle = 0.39779$  and  $\langle s_{i \in B}^z \rangle = -0.29558$ . We mention that for the classical model the transition to the UUD state takes place at  $J_2 = 2$ , i.e., the order-by-disorder mechanism [56, 57] leads to a shift of the transition to the collinear UUD state to smaller values of  $J_2$ . Bearing in mind the Schwinger-boson mean-field study of the ground state reporting 5 ground state phases [25] it is worth to have a closer look on the details of the  $m^+(J_2)$  profile. Indeed, there are small discontinuous changes in  $m^+$  at  $J_2 \approx 0.77$ ,  $J_2 \approx 0.87$  and  $J_2 \approx 1.33$  ( $J_2 \approx 0.74$ ,  $J_2 \approx 0.83$  and  $J_2 \approx 1.35$ ) for  $N = 36$  ( $N = 30$ ), where the values at about 0.85 and 1.33 are close to transition points reported in [25]. We also mention that below  $J_2 \approx 0.77$  the spins on B-sites become weakly coupled to the neighboring A-site spins, whereas the nearest-neighbor correlations on the  $J_1$  bonds asymptotically approach the value of the square-plaquette singlet ground state (see the right inset in Fig. 1), i.e., the system enters a plaquette ground-state phase at low values of  $J_2$ .

For the low-temperature thermodynamics the spin gap (singlet-triplet gap)  $\Delta_t$  as well as the singlet-singlet gap  $\Delta_s$  are relevant. Corresponding data are shown for  $N = 30$ ,  $N = 36$  and  $N = 42$  in Fig. 2. Our data provide

evidence that there is a finite spin gap  $\Delta_t$  in the region between  $J_2 \approx 0.77$  ( $J_2 \approx 0.74$ ) and  $J_2 \approx 1.65$  ( $J_2 \approx 1.65$ ) for  $N = 36$  ( $N = 30$ ). We notice only a small finite-size dependence of the spin gap away from  $J_2 = 1$ , whereas in the vicinity of  $J_2 = 1$  it shrinks with increasing  $N$ . However, it is known that  $\Delta_t$  remains finite at  $J_2 = 1$  for  $N \rightarrow \infty$  [29]. The vanishing of the spin gap at  $J_2 \approx 0.77$  coincides with the above reported value at which a small discontinuous change in  $m^+$  occurs, whereas the closing of the spin gap at  $J_2 \approx 1.65$  is related to the emergence of a ferrimagnetic ground state. Thus,  $m^+$  as well as  $\Delta_t$  yield indications for ground-state phase transitions between a gapped and a gapless phase. A similar behavior was found in Ref. [25], where, however, the region of the gapped phase is  $0.84 \leq J_2 \leq 1.27$ . While  $\Delta_t$  determines the low-temperature behavior of the susceptibility  $X$ , the existence of low-lying singlet excitations within the spin gap, i.e.,  $\Delta_s < \Delta_t$ , is crucial for the low-temperature behavior of the specific heat  $C$ . From Fig. 2 it is obvious that in the whole region with a finite spin gap we have  $\Delta_s < \Delta_t$ . As for the balanced model  $J_1 = J_2 = 1$  there are a number of singlets within the spin gap. The details of their energy distribution will determine the temperature profile of  $C$  at very low  $T$ .

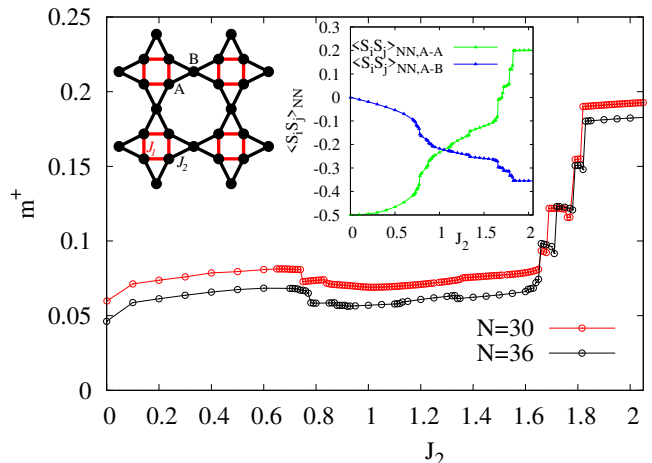


Figure 1. Main panel: Order parameter  $m^+$  as defined in Eq. (3) of the spin-1/2  $J_1$ - $J_2$  SKHAF ( $N = 30$  and  $36$ ) as a function of  $J_2$ . Left inset: Sketch of the square-kagome lattice. Here A and B label the two non-equivalent sites and  $J_1$  and  $J_2$  label the two non-equivalent nearest-neighbor bonds. Right inset: Nearest-neighbor spin-spin correlation for  $N = 36$ :  $\langle \mathbf{s}_i \cdot \mathbf{s}_j \rangle_{NN,A-A} = (\langle \mathbf{s}_0 \cdot \mathbf{s}_1 \rangle + \langle \mathbf{s}_0 \cdot \mathbf{s}_3 \rangle)/2$  and  $\langle \mathbf{s}_i \cdot \mathbf{s}_j \rangle_{NN,A-B} = (\langle \mathbf{s}_0 \cdot \mathbf{s}_4 \rangle + \langle \mathbf{s}_1 \cdot \mathbf{s}_4 \rangle)/2$ , see Fig. 12 for the numbering of sites.

### B. Thermodynamic properties of the SKHAF on finite lattices of $N = 30$ and $N = 36$ sites

Let us now consider the finite-temperature properties of the model. In what follows we discuss the Wilson ratio

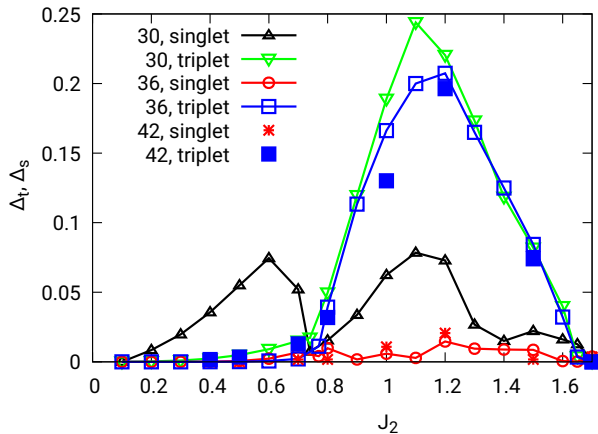


Figure 2. Singlet-triplet and singlet-singlet gaps  $\Delta_t$  and  $\Delta_s$  of the spin-1/2  $J_1$ - $J_2$  SKHAF ( $N = 30$  and  $36$ ) as a function of  $J_2$ . For a few values of  $J_2$  data for  $N = 42$  are added.

$P$ , the specific heat  $C$ , the entropy  $S$ , and the uniform susceptibility  $X$ .

The modified Wilson ratio is defined as [58, 59]

$$P(T) = 4\pi^2 TX / (3NS). \quad (4)$$

It is a measure of the ratio of the density of magnetic excitations with  $M > 0$  and the density of *all* excitations including singlet excitations with  $M = 0$ .

As shown for the KHAF [58, 59] and for the balanced SKHAF [30] a vanishing  $P$  as temperature  $T \rightarrow 0$  is a hallmark of a quantum spin-liquid ground state with dominating singlet excitations at low  $T$ . In contrast, for quantum spin models with semi-classical magnetic ground-state order, such as the square-lattice Heisenberg antiferromagnet, the Wilson ratio diverges according to a power-law [58, 59]. We show the modified Wilson ratio in Fig. 3. For  $J_2 = 0.8, 0.9, 1.0, 1.1, 1.2, 1.3, 1.4, 1.5$  singlet excitations are noticeably below the first triplet excitation. As a result there is an obvious downturn of  $P$  as  $T \rightarrow 0$ . Also the upturn of  $P$  as  $T \rightarrow 0$  for  $J_2 = 1.7$  and  $1.8$  (ferrimagnetic ground state) is evident. More subtle is the situation for  $J_2 < 0.8$ , where the plaquette ground-state phase emerges. Here the low-lying spectrum is dominated by the weakly coupled spins on the B sites, which leads to a maximum in  $P$  at low temperatures, see Fig. 3(b). This behavior can be understood by considering the ground state in the limit of decoupled B spins, i.e., for  $J_2 = 0$ . In this limit we get a size independent Wilson ratio  $P_0 = \lim_{T \rightarrow 0} P = \pi^2 / (3 \ln 2) = 4.74628$ . Obviously, the height of the low-temperature maximum in  $P$  approaches  $P_0$  as decreasing  $J_2$ . At very low  $T$  the Wilson ratio approaches a constant value of about  $P \approx 2$ . (Note, however, that our FTLM is not appropriate to get accurate data precisely at  $T = 0$ , because in the limit of very weakly coupled B spins very tiny energy differences appear in the low-energy spectrum.) As reported in Ref. [58] this behavior corresponds to a gapless

spin liquid; in particular, for the one-dimensional  $s = 1/2$  Heisenberg antiferromagnet (Bethe chain)  $P_0$  is exactly 2 [58, 60].

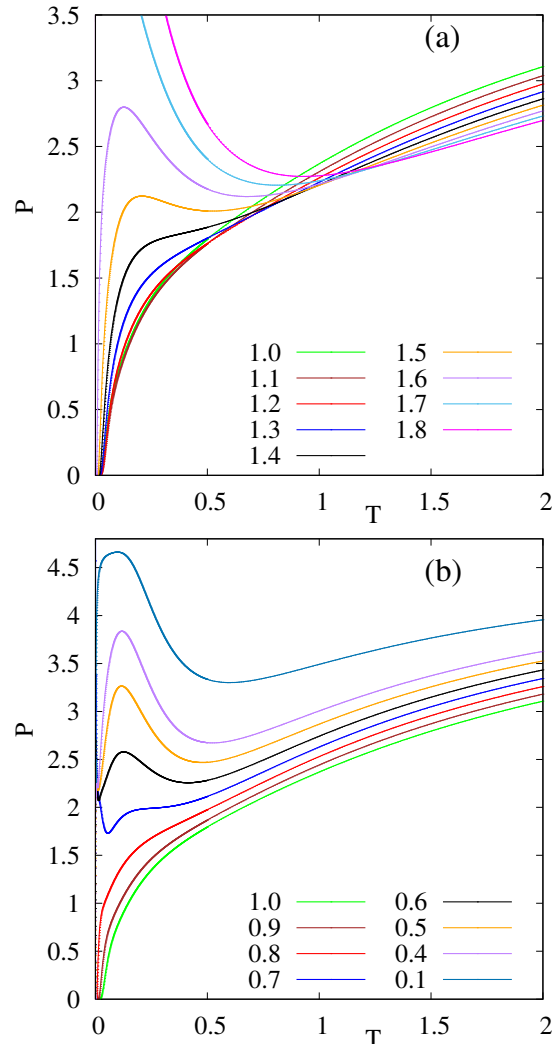


Figure 3. Modified Wilson ratio  $P(T)$ , cf. Eq. (4), of the spin-1/2  $J_1$ - $J_2$  SKHAF ( $N = 36$ ). (a)  $J_2 \geq 1.0$ , (b)  $J_2 \leq 1.0$ .

Let us now discuss the specific heat  $C(T)$ , the entropy  $S(T)$  and the uniform susceptibility  $X(T)$ . We use a logarithmic temperature scale which makes the low-temperature features transparent, see Figs. 4, 6, and 7. In panels (a) we show data for  $J_2 \geq 1$  and in panels (b) for  $J_2 \leq 1$ . In all these figures we also show the corresponding data for the balanced model [30] which may serve as benchmark data. The typical main maximum is related to the magnitudes of  $J_1$  and  $J_2$ . Its position  $T_{\max}$  and its height  $C_{\max}/N$  exhibit a quite regular behavior, see Fig. 5 (a) and (b).

From Fig. 5 it is also evident that  $T_{\max}$  and  $C_{\max}/N$  are equal for  $N = 30$  and  $36$  for all values of  $J_2$ , i.e., the main maximum in  $C(T)/N$  is not affected by finite-size effects, see also Fig. 15 in Appendix B. For all values of  $J_2$

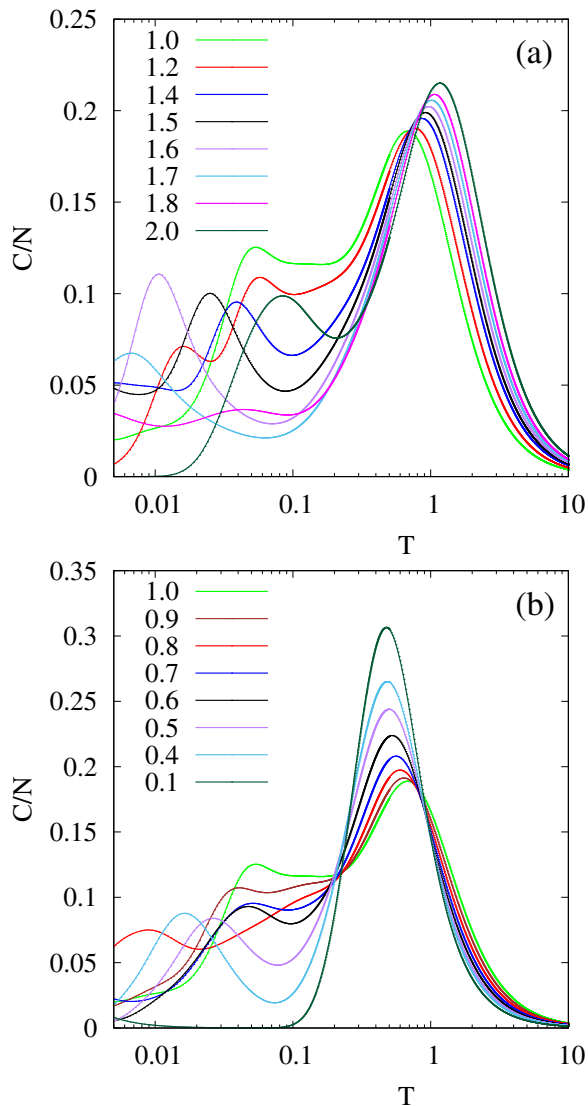


Figure 4. Specific heat  $C/N$  of the spin-1/2  $J_1$ - $J_2$  SKHAF for  $N = 36$ . (a)  $J_2 \geq 1.0$ , (b)  $J_2 \leq 1.0$ .

shown in Fig. 4 the temperature profile exhibits a low-temperature maximum below the main maximum that indicates an extra-low energy scale. Though, we show in Fig. 4 only data for  $N = 36$  this feature is present also for  $N = 30$  and  $N = 42$ , cf. Fig. 15 in Appendix B. Since the  $C(T)$  curves for  $N = 30, 36, 42$  coincide down to temperatures where this particular low- $T$  feature emerges, we may argue that this characteristic survives for  $N \rightarrow \infty$  either as an extra maximum or a shoulder below the main maximum. An additional information on the finite-size dependence of the low- $T$  part of  $C(T)$  is given in Fig. 5, where we show the position  $T_{\min}$  [panel (c)] and the depth  $C_{\min}/N$  of the minimum [panel (d)] in  $C(T)$  below the main maximum. The good agreement of the data for  $N = 30$  and  $36$  is obvious. The special values of  $T_{\min}$  and  $C_{\min}/N$  found for  $J_2 = 0.8$  might be attributed to the

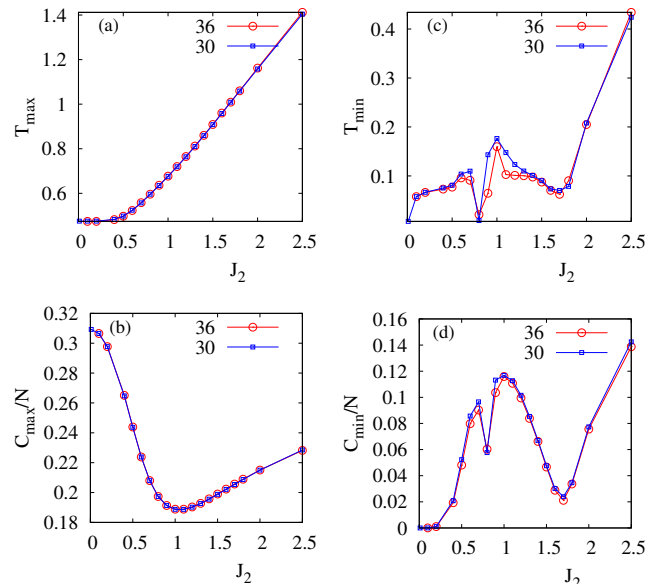


Figure 5. Features of the main maximum and the minimum below the main maximum in the temperature profile of the specific heat  $C(T)/N$  of the spin-1/2  $J_1$ - $J_2$  SKHAF ( $N = 30$  and  $N = 36$ ). (a) Position  $T_{\max}$  and (b) height  $C_{\max}/N$  of the main maximum. (c) Position  $T_{\min}$  and (d) depth  $C_{\min}/N$  of the minimum.

proximity to the transition point to the plaquette phase. Interestingly, there is also a double-maximum profile in  $C(T)$  for  $J_2 = 1.8$  and  $2.0$ , where the ground state is ferrimagnetic. Only beyond  $J_2 \sim 3$  we get a  $C(T)$  profile with only one maximum, see Fig. 14 in Appendix B. Let us finally mention that for some values of  $J_2$  there is even some additional structure at very low  $T \lesssim 0.02$  which most likely can be attributed to finite-size effects.

In highly frustrated quantum magnets we may have a high density of states at low excitation energies [30, 34, 61]. To shed light on the density of low-lying eigenstates we present the entropy  $S(T)/N$  in Fig. 6. We observe, that already at  $T \sim 0.2$  about 50% of the maximum entropy  $S(T \rightarrow \infty) = N \ln 2$  is acquired. Note that for the unfrustrated square-lattice Heisenberg antiferromagnet the corresponding value at  $T \sim 0.2$  is only about 10%, cf. Ref. [34]. Moreover, there is a change in the curvature or even a plateau-like feature in the  $S(T)$  profile below this temperature. In particular, for  $J_2 \lesssim 0.7$  we see such a plateau at  $S/(N \ln 2) \sim 0.1$  which can be attributed to a high density of states caused by the weakly coupled B spins in this parameter region. For some values of  $J_2$  (e.g. for  $J_2 = 2.0$  and  $1.2$ ) there is a finite value of  $S(T = 0)/N$  due a degeneracy of the ground state. However,  $S(T = 0)/N$  will become zero as  $N \rightarrow \infty$ . For more information on finite-size effects, see Fig. 16 in Appendix B, where data for  $N = 30$ ,  $N = 36$  and  $N = 42$  are compared.

Next we turn to the zero-field susceptibility  $X$  displayed in Fig. 7. For  $J_2$  values where we have a finite

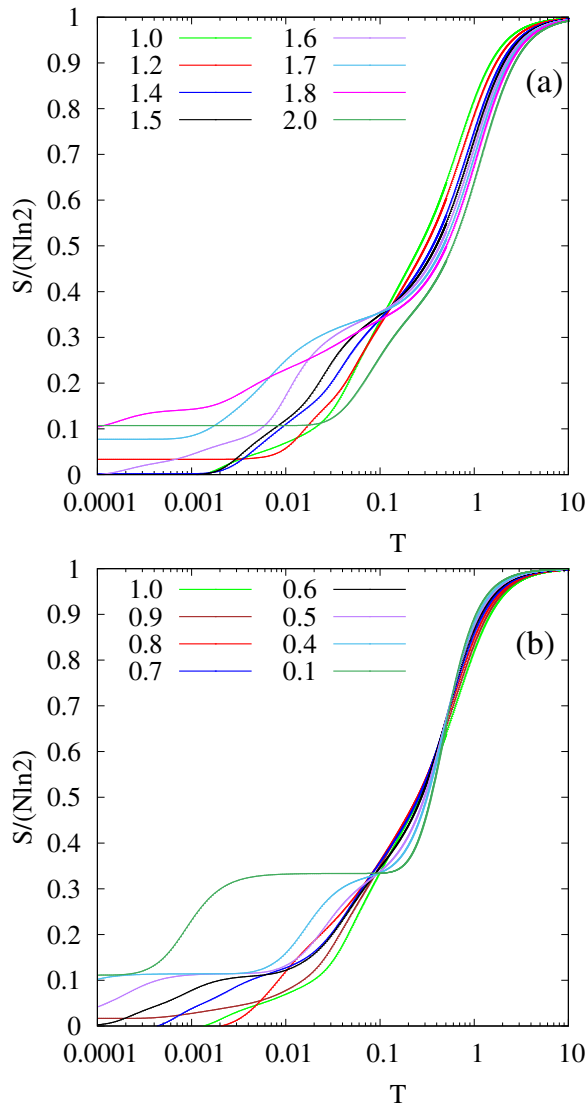


Figure 6. Entropy  $S/N$  of the spin-1/2  $J_1$ - $J_2$  SKHAF for  $N = 36$ . (a)  $J_2 \geq 1.0$ , (b)  $J_2 \leq 1.0$ . Note that the finite entropy at  $T = 0$  for  $J_2 = 1.8$  and  $2.0$  is caused by the ferrimagnetic multiplet and by an accidental degeneracy of the ground state for some other values of  $J_2$ .

singlet-triplet gap  $\Delta_t$ , see Fig. 2,  $X$  exhibits an exponentially activated low-temperature behavior and there is a maximum in  $X(T)$ . Its position  $T_{\max}$  and its height  $X_{\max}/N$  exhibit a quite regular behavior, and the finite-size effects in  $T_{\max}$  and  $X_{\max}/N$  are small, see Fig. 8. (For more information on finite-size effects, see Fig. 17 in Appendix B, where data for  $N = 30$ ,  $N = 36$ , and  $N = 42$  are compared.) Around  $J_2 = 1$  the position  $T_{\max}$  is largest, although, it is still at a pretty low temperature compared to  $T_{\max} = 0.935$  for the square-lattice Heisenberg antiferromagnet [62, 63], which demonstrates the crucial role of frustration also for the susceptibility. It is also obvious that  $T_{\max}$  is directly related to the spin gap  $\Delta_T$ , compare Fig. 8(a) and Fig. 2. Increas-

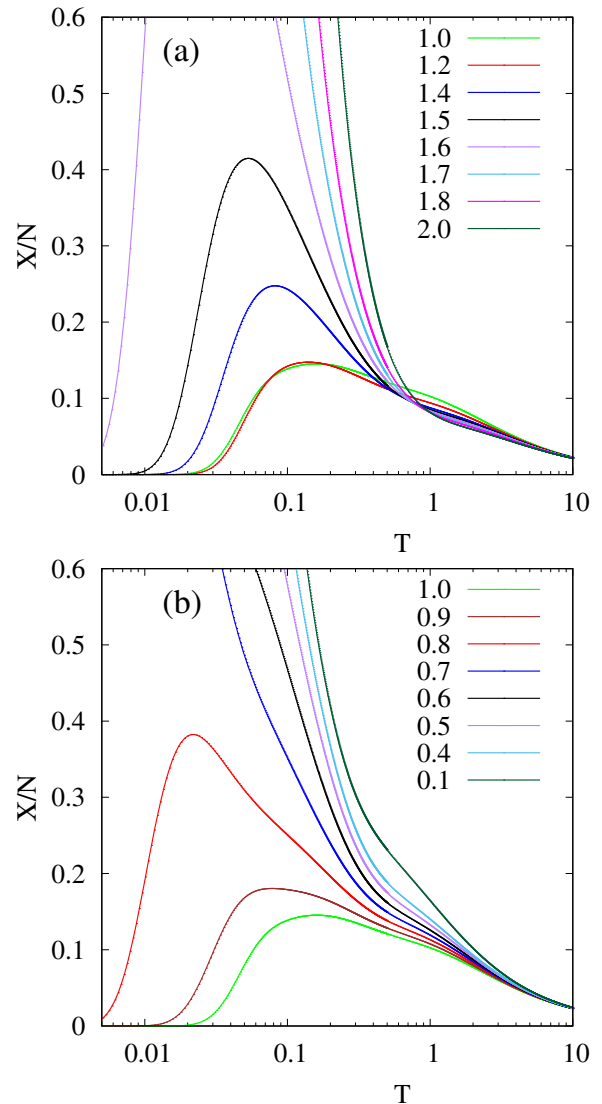


Figure 7. Susceptibility  $X/N$  of the spin-1/2  $J_1$ - $J_2$  SKHAF for  $N = 36$ . (a)  $J_2 \geq 1.0$ , (b)  $J_2 \leq 1.0$ .

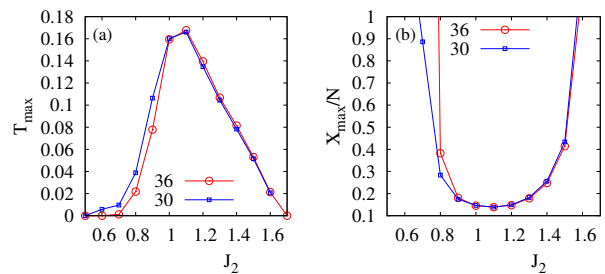


Figure 8. Features of the maximum in the temperature profile of the susceptibility  $X(T)/N$  of the spin-1/2  $J_1$ - $J_2$  SKHAF ( $N = 30$  and  $N = 36$ ). (a) Position  $T_{\max}$  of the maximum. (b) Height  $X_{\max}/N$  of the maximum.

ing  $J_2$  towards the transition to the ferrimagnetic ground

state naturally leads to a diminishing of  $T_{\max}$  and an increase of  $X_{\max}/N$ . At  $J_2 \sim 1.65$  we get  $T_{\max} = 0$  and  $X_{\max}/N \rightarrow \infty$ .

A similar behavior can be observed for decreasing  $J_2$  towards  $J_2 = 0$ . Again the singlet-triplet gap  $\Delta_t$  becomes smaller and it is effectively zero below  $J_2 \sim 0.77$  (plaquette ground-state phase), i.e.,  $T_{\max}$  approaches zero. However, here the weakly coupled spins on the B sites lead to extremely low-lying magnetic and non-magnetic excitations. In fact, we find that for the finite systems considered here the ground state is still a non-magnetic singlet but magnetic excitations dominate the  $X(T)/N$  profile down to very low  $T$ . Thus, the susceptibility indeed vanishes at  $T = 0$ , but  $X(T)/N$  approaches zero only at  $T \sim 10^{-4}$ ,  $10^{-5}$ ,  $10^{-9}$  for  $J_2 = 0.7, 0.5, 0.1$ , respectively.

### C. Field-dependent properties

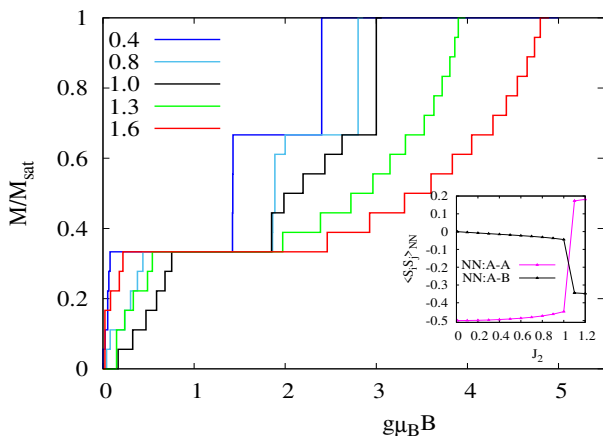


Figure 9. Main panel: Zero-temperature magnetization curves of the  $J_1$ - $J_2$  SKHAF with  $N = 36$  sites and selected values of  $J_2$ . Inset: Nearest-neighbor correlation functions  $\langle \mathbf{s}_i \cdot \mathbf{s}_j \rangle_{NN,A-A}$  and  $\langle \mathbf{s}_i \cdot \mathbf{s}_j \rangle_{NN,A-B}$  in the  $1/3$  plateau state.

The magnetization process of strongly frustrated quantum magnets exhibits a number of interesting features, such as plateaus and jumps [64]. Previous studies for the balanced model [13, 14, 29, 30, 65] report on wide plateaus at  $1/3$  and  $2/3$  of the saturation magnetization  $M_{\text{sat}}$ . Moreover, there is the typical macroscopic jump to saturation due to the presence of independent localized multi-magnon ground states stemming from a flat one-magnon band [15, 66–68].

Let us first present the zero-temperature magnetization curve for selected values of  $J_2$ , see Fig. 9. Both plateaus as well as the jump to saturation known from the balanced model are present for all values  $J_2 \leq 1$ , whereas for  $J_2 > 1$  the jump and the related preceding  $2/3$  plateau are missing. For  $J_2 \leq 1$  both plateau states are non-classical valence-bond states, cf. Refs. [13, 29, 30, 65],

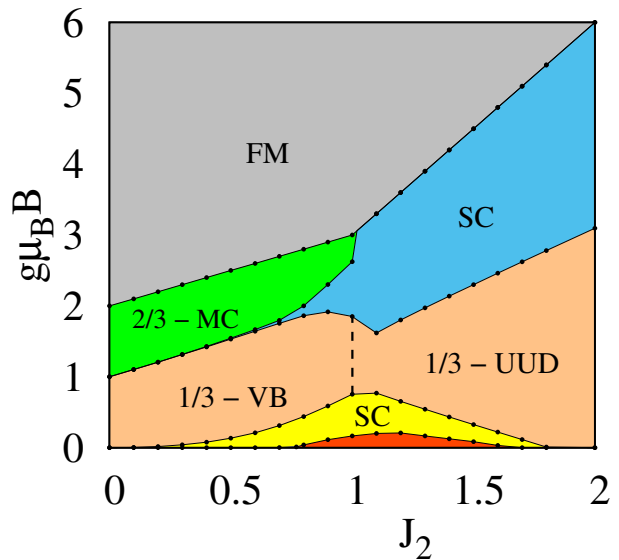


Figure 10. Sketch of the zero-temperature  $J_2$ - $B$  phase diagram. FM: ferromagnetic,  $1/3$ -VB:  $M = M_{\text{sat}}/3$  (valence-bond state),  $1/3$ -UUD:  $M = M_{\text{sat}}/3$  (up-up-down state),  $2/3$ -MC:  $M = 2M_{\text{sat}}/3$  (magnon crystal), SC: spin canting above and below the  $1/3$  plateau, red area:  $M = 0$  (gapped phase).

where the upper plateau state is the exactly known magnon-crystal product state, i.e., spins on the  $B$  sites are fully polarized and the  $A$ -spins on a square plaquette occupy the lowest triplet eigenstate of the square plaquette with  $S_{\text{plaq}}^z = 1$ , for an illustration of this state, see, e.g., Fig. 2a in Ref. [69]. For  $J_2 \lesssim 0.7$  the transition between the two plateaus becomes steplike. The jump to saturation as well as the magnon-crystal product state are related to the flat one-magnon band which is the lowest one for  $J_2 \leq 1$ . In contrast, for  $J_2 > 1$ , the flat one-magnon band is not the lowest one, and, therefore the flat-band related features are not present in the magnetization curve. However, the flat-band related localized multi-magnon states including the magnon crystal are still eigenstates living now as quantum scar states somewhere in the middle of the spectrum [26].

The valence-bond state of the lower plateau is not exactly known but it is approximately described by a product state with fully polarized spins on the  $B$  sites and a singlet state of the  $A$ -spins on a square, see the inset in Fig. 9, where the spin-spin correlations  $\langle \mathbf{s}_i \cdot \mathbf{s}_j \rangle_{NN,A-A}$  and  $\langle \mathbf{s}_i \cdot \mathbf{s}_j \rangle_{NN,A-B}$  in the  $1/3$  plateau state are shown. On the other hand, for  $J_2 > 1$  the  $1/3$  plateau state is semi-classical, namely it is the ferrimagnetic UUD state, cf. Sec. III A and see the inset in Fig. 9.

Using the entire set of calculated magnetization curves for  $N = 36$  (which includes altogether 22  $J_2$  values in the region  $0 \leq J_2 \leq 2$ ) we can construct the  $J_2$ - $B$  phase diagram shown in Fig. 10. The saturation magnetization (uppermost line) is given by  $g\mu_B B_{\text{sat}} = 2 + J_2$  for  $J_2 \leq 1$

and  $g\mu_B B_{\text{sat}} = 3J_2$  for  $J_2 \geq 1$ , and it is size-independent. But also for the other phase boundaries derived from numerical data, the finite-size effects are very small, see Fig. 13 in appendix B.

For elevated temperatures the experimental detection of plateaus may become intricate, because often there is a fast melting of plateaus and jumps, i.e., they are smeared out already at pretty low  $T$ , see, e.g., Refs. [65, 70]. Therefore, to detect plateaus and jumps in experiments the differential susceptibility  $X(T, B) = dM(T, B)/d(g\mu_B B)$  as a function of  $B$  measured at various  $T$  is more suitable, cf., e.g., Ref. [71]. Magnetization plateaus show up as pronounced minima in  $X(B)$ , however, requiring sufficiently low temperatures. On the other hand, a jump of the magnetization leads to a high peak in  $X(B)$  at low  $T$ .

We present the influence of the temperature on the magnetization curve  $M(B)$  and on the differential susceptibility  $X(B)$  in Fig. 11 for selected values of  $J_2$ . We observe, that the melting process is most rapid for  $J_2 \sim 1$ , whereas for small and large  $J_2$  the plateaus and the jumps are still well visible at  $T = 0.2$ . We notice that the oscillations present for  $J_2 \geq 1$  at  $T = 0.05$  (green curves) above the  $1/3$  plateau are finite-size effects.

#### IV. SUMMARY AND CONCLUSIONS

In our study we performed numerical calculations of thermodynamic quantities such as the magnetization  $M(T)$ , the specific heat  $C(T)$ , the entropy  $S(T)$  and the susceptibility  $X(T)$  for the  $J_1$ - $J_2$  spin-half square-kagome Heisenberg antiferromagnet (SKHAF) by using the finite-temperature Lanczos method (FTLM) applied to finite lattices of  $N = 30$ ,  $N = 36$  and  $N = 42$  sites. Since the SKHAF exhibits two non-equivalent nearest-neighbor bonds, the extension of previous studies [16, 30], which were restricted to  $J_1 = J_2$ , on the generalized model with  $J_1 \neq J_2$  is natural with respect to experimental realization of the SKHAF, see Refs. [7–10]. Moreover, the generalized model may serve as a model allowing to tune the competition of antiferromagnetic bonds in a highly frustrated spin system.

The exact-diagonalization data for the ground state indicate magnetic disorder in a wide range of  $J_2/J_1$  ratios. Only for  $J_2 \gtrsim 1.65J_1$  the ground state features ferrimagnetic order. In the region  $0.77 \lesssim J_2/J_1 \leq 1.65$  the low-temperature thermodynamics is determined by a finite singlet-triplet gap with low-lying singlets within this gap. Therefore, the susceptibility decays exponentially to zero as temperature  $T \rightarrow 0$ , while the specific heat exhibits an extra maximum at low  $T$  related to the singlets. For smaller values of  $J_2/J_1 \lesssim 0.7$  the ground state becomes a plaquette ground state with weakly coupled spins on B sites which become asymptotically decoupled as  $J_2/J_1 \rightarrow 0$ . As a result, the entropy acquires already a large amount at very low temperatures.

In non-zero magnetic field  $B$  we find well pronounced

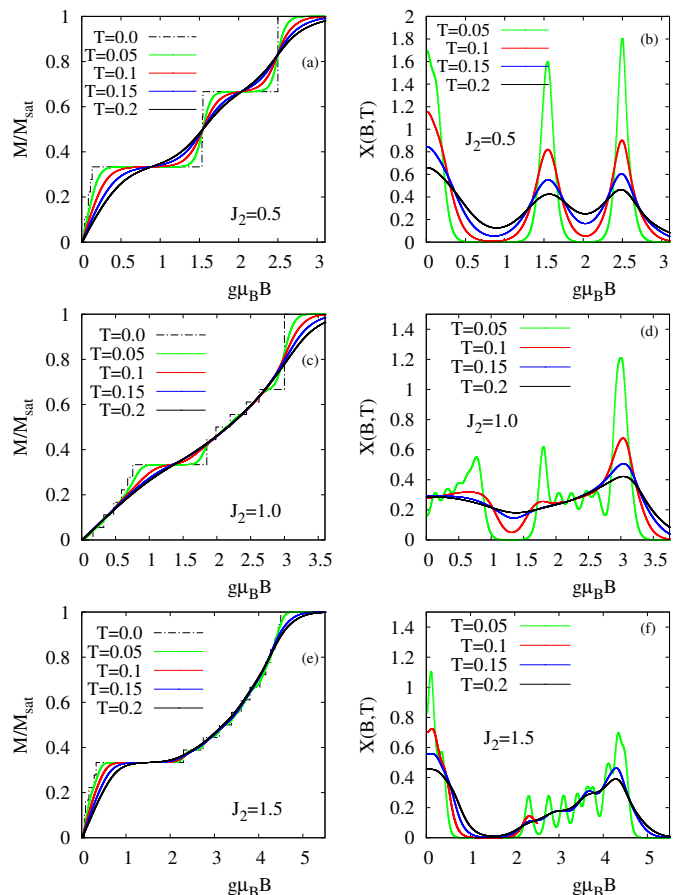


Figure 11. Left panels: Finite temperature magnetization curves  $M(T, B)$  of the  $J_1$ - $J_2$  SKHAF with  $N = 36$  sites for selected values of  $J_2$ . Right panels: Corresponding data of the differential susceptibility  $X(T, B) = dM(T, B)/d(g\mu_B B)$ .

plateaus at  $1/3$  and  $2/3$  of the saturation magnetization and a jump from the  $2/3$  plateau to saturation in the whole region  $0 \leq J_2/J_1 \leq 1$ , whereas for  $J_2/J_1 > 1$  only the  $1/3$  plateau is present. At low and moderate temperature the plateaus are reflected as minima in the differential susceptibility  $X(B) = dM(B)/d(g\mu_B B)$  and a jump is seen as a peak in  $X(B)$ .

Bearing in mind the numerous studies of the low-energy physics of the related kagome Heisenberg antiferromagnet we argue that our work may also stimulate other studies using alternative techniques, such as tensor network methods, DMRG, numerical linked cluster expansion or Green's function techniques [29, 72–77].

#### ACKNOWLEDGMENT

This work was supported by the Deutsche Forschungsgemeinschaft (DFG RI 615/25-1 and SCHN 615/28-1). Computing time at the Leibniz Center in Garching (project pr62to) is gratefully acknowledged.

### Appendix A: Finite square-kagome lattices used for the exact diagonalization and the finite-temperature Lanczos method

Here we provide the finite lattices studied in our paper, see Fig. 12.

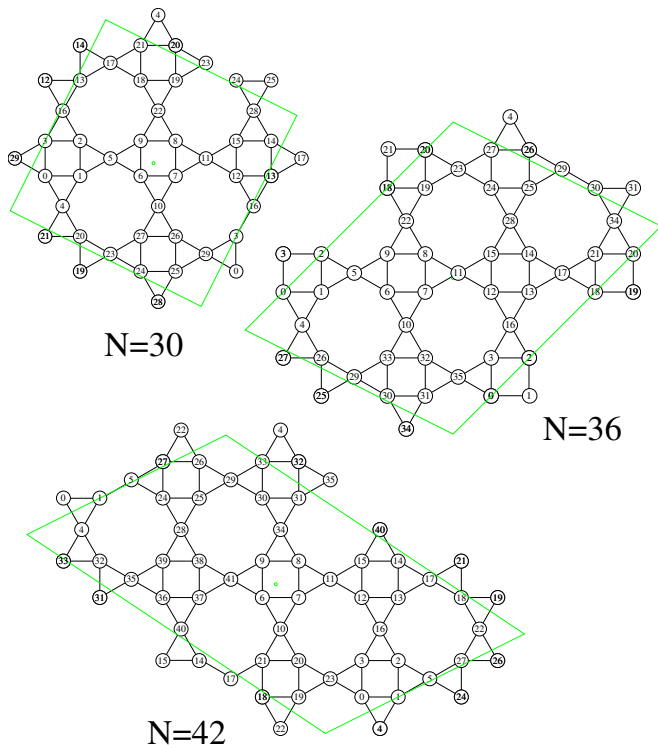


Figure 12. Finite square-kagome lattices of  $N = 30$ ,  $N = 36$  and  $N = 42$  sites.

### Appendix B: Finite-size effects

Here we present data for the widths of the  $1/3$  and  $2/3$  plateaus (Fig. 13) and show the specific heat for large values of  $J_2$  (Fig. 14). Moreover, we provide additional information on finite-size effects for the specific heat  $C(T)$  (Fig. 15), the entropy  $S(T)$  (Fig. 16) and the susceptibility  $X(T)$  (Fig. 17) by comparing data for  $N = 30$ ,  $N = 36$ ,  $N = 42$ .

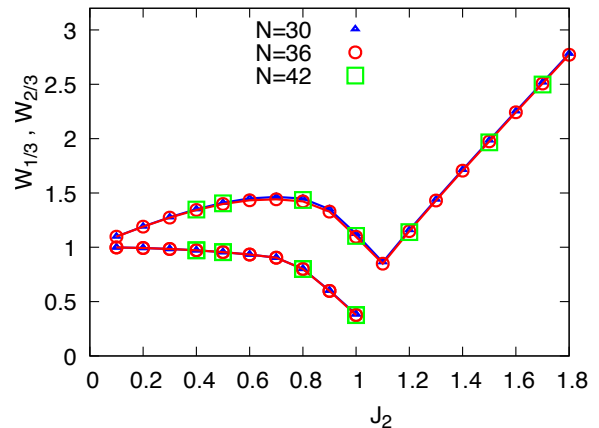


Figure 13. Widths  $W_{1/3} = g\mu_B(B_{2,1/3} - B_{1,1/3})$  of the  $1/3$  plateau and  $W_{2/3} = g\mu_B(B_{2,2/3} - B_{1,2/3})$  of the  $2/3$  plateau of the  $J_1$ - $J_2$  SKHAF for  $N = 30$ ,  $N = 36$  and  $N = 42$ .

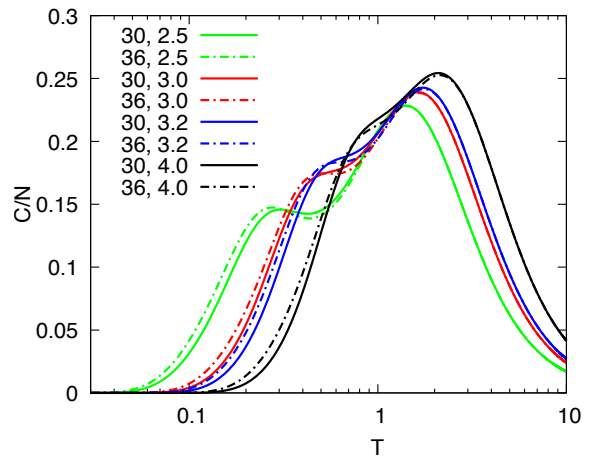


Figure 14. Specific heat per site  $C/N$  for  $N = 30$  (dashed lines) and  $N = 36$  (solid lines) for large values of  $J_2$ . Note that in a wide temperature range the corresponding curves for  $N = 30$  and  $36$  coincide.

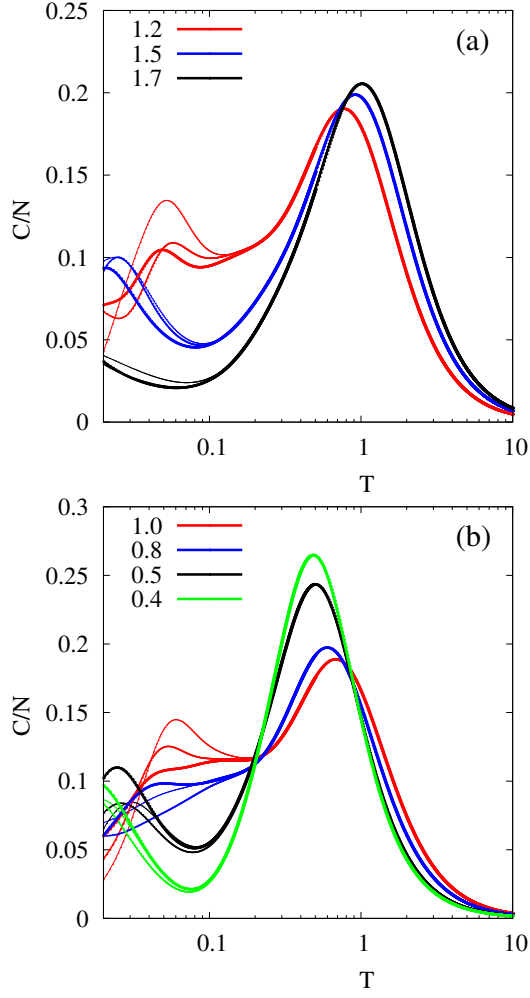


Figure 15. Specific heat per site  $C/N$  for  $N = 30$  (thin),  $N = 36$  (middle) and  $N = 42$  (thick). (a)  $J_2 > 1.0$ , (b)  $J_2 \leq 1.0$ . Note that in a wide temperature range the corresponding curves for  $N = 30$ , 36 and  $N = 42$  coincide.

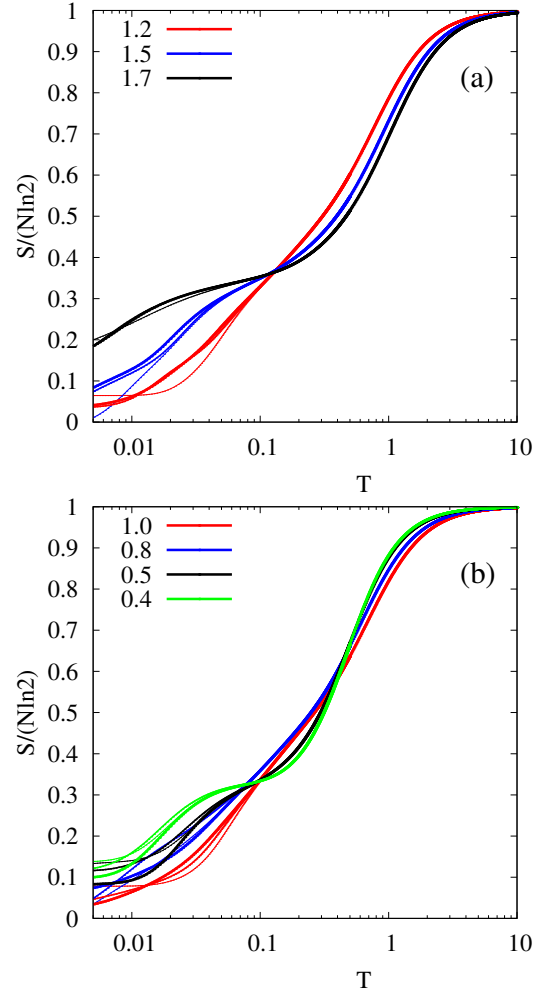


Figure 16. Entropy per site  $S/N$  for  $N = 30$  (thin),  $N = 36$  (middle) and  $N = 42$  (thick). (a)  $J_2 > 1.0$ , (b)  $J_2 \leq 1.0$ . Note that in a wide temperature range the corresponding curves for  $N = 30$ , 36 and  $N = 42$  coincide.

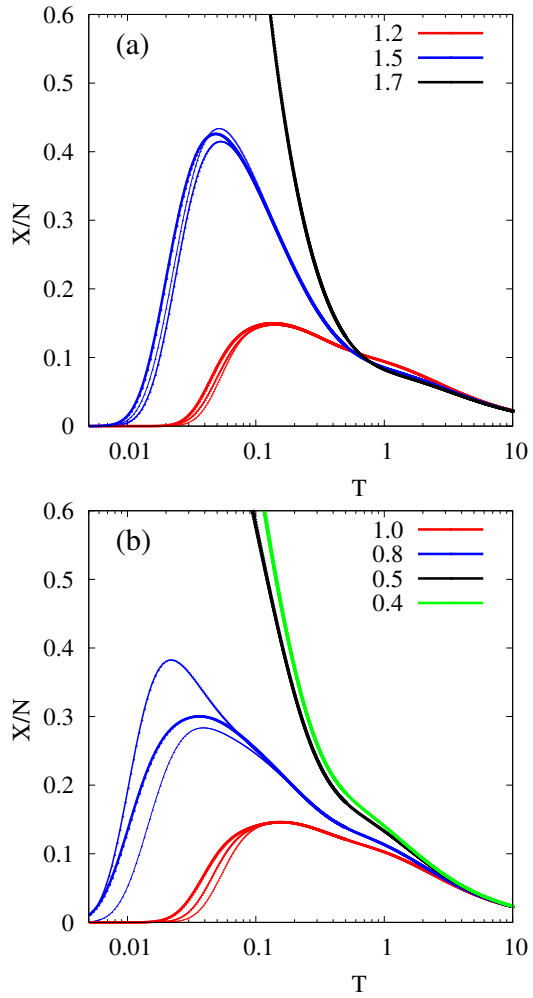


Figure 17. Susceptibility per site  $X/N$  for  $N = 30$  (thin),  $N = 36$  (middle) and  $N = 42$  (thick). (a)  $J_2 > 1.0$ , (b)  $J_2 \leq 1.0$ . Note that in a wide temperature range the corresponding curves for  $N = 30$ ,  $36$  and  $N = 42$  coincide. Only for  $J_2 = 0.8$  there is a noticeable difference around the maximum which is, however, at pretty low  $T$ .

- [1] R. Moessner, Magnets with strong geometric frustration, *Can. J. Phys.* **79**, 1283 (2001).
- [2] J. Richter, J. Schulenburg, and A. Honecker, Quantum magnetism in two dimensions: From semi-classical Néel order to magnetic disorder, *Quantum Magnetism, Lecture Notes in Physics* **645**, 85 (2004).
- [3] C. Lacroix, F. Mila, and P. Mendels, eds., *Introduction to Frustrated Magnetism* (Berlin & Heidelberg, 2010).
- [4] Spin liquids in frustrated magnets, *Nature* **464**, 199 (2010).
- [5] L. Savary and L. Balents, Quantum spin liquids, *Rep. Prog. Phys.* **80**, 016502 (2017).
- [6] P. A. McClarty, Topological magnons: A review, *Annual Review of Condensed Matter Physics* **13**, 171 (2022).
- [7] M. Fujihala, K. Morita, R. Mole, S. Mitsuda, T. Tohyama, S.-i. Yano, D. Yu, S. Sota, T. Kuwai, A. Koda, H. Okabe, H. Lee, S. Itoh, T. Hawai, T. Masuda, H. Sagayama, A. Matsuo, K. Kindo, S. Ohira-Kawamura, and K. Nakajima, Gapless spin liquid in a square-kagome lattice antiferromagnet, *Nat. Commun.* **11**, 3429 (2020).
- [8] O. V. Yakubovich, L. V. Shvanskaya, G. V. Kiriuikhina, A. S. Volkov, O. V. Dimitrova, and A. N. Vasiliev, Hydrothermal synthesis and a composite crystal structure of  $\text{Na}_6\text{Cu}_7\text{BiO}_4(\text{PO}_4)_4[\text{Cl}(\text{OH})]_3$  as a candidate for quantum spin liquid, *Inorganic Chemistry* **60**, 11450 (2021).
- [9] B. Liu, Z. Zeng, A. Xu, Y. Sun, O. Yakubovich, L. Shvanskaya, S. Li, and A. Vasiliev, Low-temperature specific-heat studies on two square-kagome antiferromagnets, *Phys. Rev. B* **105**, 155153 (2022).
- [10] M. Markina, P. Berdonosov, T. Vasilchikova, K. Zakharov, A. Murtazoev, V. Dolgikh, A. Moskvin, V. Glazkov, A. Smirnov, and A. Vasiliev, *Static and resonant properties of decorated square kagome lattice compound  $\text{KCu}_7(\text{TeO}_4)(\text{SO}_4)_5\text{Cl}$*  (2022), arXiv:2212.11623 [cond-mat.str-el].
- [11] R. Siddharthan and A. Georges, Square kagome quantum antiferromagnet and the eight-vertex model, *Phys. Rev. B* **65**, 014417 (2001).
- [12] The spin-half Heisenberg antiferromagnet on the square-kagomé lattice: Ground state and low-lying excitations, author=J. Richter and J. Schulenburg and P. Tomczak and D. Schmalfuß, year=2004, eprint=cond-mat/0411673, archiveprefix=arXiv, primaryclass=cond-mat.str-el.
- [13] J. Richter, J. Schulenburg, P. Tomczak, and D. Schmalfuß, The Heisenberg antiferromagnet on the square-kagome lattice, *Cond. Matter Phys.* **12**, 507 (2009).
- [14] H. Nakano and T. Sakai, The two-dimensional  $s = 1/2$  Heisenberg antiferromagnet on the shuriken lattice – a lattice composed of vertex-sharing triangles, *J. Phys. Soc. Jpn.* **82**, 083709 (2013).
- [15] J. Schnack, H.-J. Schmidt, J. Richter, and J. Schulenburg, Independent magnon states on magnetic polytopes, *Eur. Phys. J. B* **24**, 475 (2001).
- [16] P. Tomczak and J. Richter, Specific heat of the spin-1/2 Heisenberg antiferromagnet on square kagome lattice, *J. Phys. A: Math. Gen.* **36**, 5399 (2003).
- [17] J. Richter, O. Derzhko, and J. Schulenburg, Magnetic-field induced spin-Peierls instability in strongly frustrated quantum spin lattices, *Phys. Rev. Lett.* **93**, 107206 (2004).
- [18] I. Rousochatzakis, R. Moessner, and J. v. d. Brink, Frustrated magnetism and resonating valence bond physics in two-dimensional kagome-like magnets, *Phys. Rev. B* **88**, 195109 (2013).
- [19] O. Derzhko, J. Richter, O. Krupnitska, and T. Krokhsalskii, The square-kagome quantum Heisenberg antiferromagnet at high magnetic fields: The localized-magnon paradigm and beyond, *Low Temp. Phys.* **40**, 513 (2014).
- [20] A. Ralko and I. Rousochatzakis, Resonating-valence-bond physics is not always governed by the shortest tunneling loops, *Phys. Rev. Lett.* **115**, 167202 (2015).
- [21] H. Nakano, Y. Hasegawa, and T. Sakai, Magnetization jump in the magnetization process of the spin-1/2 Heisenberg antiferromagnet on a distorted square-kagome lattice, *J. Phys. Soc. Jpn.* **84**, 114703 (2015).
- [22] O. Derzhko, J. Richter, and M. Maksymenko, Strongly correlated flat-band systems: The route from Heisenberg spins to Hubbard electrons, *Int. J. Mod. Phys. B* **29**, 1530007 (2015).
- [23] Y. Hasegawa, H. Nakano, and T. Sakai, Metamagnetic jump in the spin- $\frac{1}{2}$  antiferromagnetic Heisenberg model on the square kagome lattice, *Phys. Rev. B* **98**, 014404 (2018).
- [24] K. Morita and T. Tohyama, Magnetic phase diagrams and magnetization plateaus of the spin-1/2 antiferromagnetic Heisenberg model on a square-kagome lattice with three nonequivalent exchange interactions, *J. Phys. Soc. Jpn.* **87**, 043704 (2018).
- [25] T. Lugan, L. D. C. Jaubert, and A. Ralko, Topological nematic spin liquid on the square kagome lattice, *Phys. Rev. Research* **1**, 033147 (2019).
- [26] P. A. McClarty, M. Haque, A. Sen, and J. Richter, Disorder-free localization and many-body quantum scars from magnetic frustration, *Phys. Rev. B* **102**, 224303 (2020).
- [27] Y. Kuno, T. Mizoguchi, and Y. Hatsugai, Flat band quantum scar, *Phys. Rev. B* **102**, 241115(R) (2020).
- [28] N. Astrakhantsev, F. Ferrari, N. Niggemann, T. Müller, A. Chauhan, A. Kshetrimayum, P. Ghosh, N. Regnault, R. Thomale, J. Reuther, T. Neupert, and Y. Iqbal, Pinwheel valence bond crystal ground state of the spin- $\frac{1}{2}$  Heisenberg antiferromagnet on the shuriken lattice, *Phys. Rev. B* **104**, L220408 (2021).
- [29] P. Schmoll, A. Kshetrimayum, J. Naumann, J. Eisert, and Y. Iqbal, Tensor network study of the spin- $\frac{1}{2}$  Heisenberg antiferromagnet on the shuriken lattice, *Phys. Rev. B* **107**, 064406 (2023).
- [30] J. Richter, O. Derzhko, and J. Schnack, Thermodynamics of the spin-half square kagome lattice antiferromagnet, *Phys. Rev. B* **105**, 144427 (2022).
- [31] P. Lecheminant, B. Bernu, C. Lhuillier, L. Pierre, and P. Sindzingre, Order versus disorder in the quantum Heisenberg antiferromagnet on the kagome lattice using exact spectra analysis, *Phys. Rev. B* **56**, 2521 (1997).
- [32] C. Waldtmann, H.-U. Everts, B. Bernu, C. Lhuillier, P. Sindzingre, P. Lecheminant, and L. Pierre, First excitations of the spin 1/2 Heisenberg antiferromagnet on the kagomé lattice, *Eur. Phys. J. B* **2**, 501 (1998).
- [33] A. M. Läuchli, J. Sudan, and R. Moessner,  $s = \frac{1}{2}$  kagome Heisenberg antiferromagnet revisited, *Phys. Rev. B* **100**, 155142 (2019).

- [34] J. Schnack, J. Schulenburg, and J. Richter, Magnetism of the  $N = 42$  kagome lattice antiferromagnet, *Phys. Rev. B* **98**, 094423 (2018).
- [35] Z. Zeng, X. Ma, S. Wu, H.-F. Li, Z. Tao, X. Lu, X.-h. Chen, J.-X. Mi, S.-J. Song, G.-H. Cao, G. Che, K. Li, G. Li, H. Luo, Z. Y. Meng, and S. Li, Possible Dirac quantum spin liquid in the kagome quantum antiferromagnet  $\text{YCu}_3(\text{OH})_6\text{Br}_2[\text{Br}_x(\text{OH})_{1-x}]$ , *Phys. Rev. B* **105**, L121109 (2022).
- [36] A. Läuchli, Numerical simulations of frustrated systems, in *Introduction to Frustrated Magnetism*, edited by C. Lacroix, P. Mendels, and F. Mila (Springer, Berlin, Heidelberg, 2011) p. 34.
- [37] J. Richter, J. Schulenburg, A. Honecker, and D. Schmalfuß, Absence of magnetic order for the spin-half Heisenberg antiferromagnet on the star lattice, *Phys. Rev. B* **70**, 174454 (2004).
- [38] J. Schulenburg, *spinpack 2.56*, Magdeburg University (2017).
- [39] J. Richter and J. Schulenburg, The spin-1/2  $J_1 - J_2$  Heisenberg antiferromagnet on the square lattice: Exact diagonalization for  $N = 40$  spins, *Eur. Phys. J. B* **73**, 117 (2010).
- [40] J. Jaklič and P. Prelovšek, Lanczos method for the calculation of finite-temperature quantities in correlated systems, *Phys. Rev. B* **49**, 5065 (1994).
- [41] A. Hams and H. De Raedt, Fast algorithm for finding the eigenvalue distribution of very large matrices, *Phys. Rev. E* **62**, 4365 (2000).
- [42] M. Aichhorn, M. Daghofer, H. G. Evertz, and W. von der Linden, Low-temperature Lanczos method for strongly correlated systems, *Phys. Rev. B* **67**, 161103(R) (2003).
- [43] J. Schnack and O. Wendland, Properties of highly frustrated magnetic molecules studied by the finite-temperature Lanczos method, *Eur. Phys. J. B* **78**, 535 (2010).
- [44] S. Sugiura and A. Shimizu, Thermal pure quantum states at finite temperature, *Phys. Rev. Lett.* **108**, 240401 (2012).
- [45] P. Prelovšek and J. Bonča, Strongly correlated systems, numerical methods (Springer, Berlin, Heidelberg, 2013) Chap. Ground State and Finite Temperature Lanczos Methods.
- [46] S. Sugiura and A. Shimizu, Canonical thermal pure quantum state, *Phys. Rev. Lett.* **111**, 010401 (2013).
- [47] B. Schmidt and P. Thalmeier, Frustrated two dimensional quantum magnets, *Phys. Rep.* **703**, 1 (2017).
- [48] E. Pavarini, E. Koch, R. Scalettar, and R. M. Martin, eds., The physics of correlated insulators, metals, and superconductors (2017) Chap. The Finite Temperature Lanczos Method and its Applications by P. Prelovšek, ISBN 978-3-95806-224-5, <http://hdl.handle.net/2128/15283>.
- [49] P. Prelovšek and J. Kokalj, Finite-temperature properties of the extended Heisenberg model on a triangular lattice, *Phys. Rev. B* **98**, 035107 (2018).
- [50] S. Okamoto, G. Alvarez, E. Dagotto, and T. Tohyama, Accuracy of the microcanonical Lanczos method to compute real-frequency dynamical spectral functions of quantum models at finite temperatures, *Phys. Rev. E* **97**, 043308 (2018).
- [51] K. Inoue, Y. Maeda, H. Nakano, and Y. Fukumoto, Canonical-ensemble calculations of the magnetic susceptibility for a spin-1/2 spherical kagome cluster with dzyaloshinskii-moriya interactions by using microcanonical thermal pure quantum states, *IEEE Transactions on Magnetism* **55**, 1 (2019).
- [52] K. Morita and T. Tohyama, Finite-temperature properties of the Kitaev-Heisenberg models on kagome and triangular lattices studied by improved finite-temperature Lanczos methods, *Phys. Rev. Research* **2**, 013205 (2020).
- [53] J. Schnack, J. Richter, and R. Steinigeweg, Accuracy of the finite-temperature Lanczos method compared to simple typicality-based estimates, *Phys. Rev. Research* **2**, 013186 (2020).
- [54] H. Schlüter, F. Gayk, H.-J. Schmidt, A. Honecker, and J. Schnack, Accuracy of the typicality approach using chebyshev polynomials, *Z. Naturforsch. A* **76**, 823 (2021).
- [55] J. Schnack, J. Schulenburg, A. Honecker, and J. Richter, Magnon crystallization in the kagome lattice antiferromagnet, *Phys. Rev. Lett.* **125**, 117207 (2020).
- [56] J. Villain, R. Bidaux, J.-P. Carton, and R. Conte, Order as an effect of disorder, *J. Phys.* **41**, 1263 (1980).
- [57] E. F. Shender, Antiferromagnetic garnets with fluctuational interacting sublattices, *JETP* **56**, 178 (1982).
- [58] P. Prelovsek, K. Morita, T. Tohyama, and J. Herbrych, Vanishing Wilson ratio as the hallmark of quantum spin-liquid models, *Phys. Rev. Research* **2**, 023024 (2020).
- [59] P. Prelovsek and J. Kokalj, Similarity of thermodynamic properties of the Heisenberg model on triangular and kagome lattices, *Phys. Rev. B* **101**, 075105 (2020).
- [60] D. C. Johnston, R. K. Kremer, M. Troyer, X. Wang, A. Klümper, S. L. Bud'ko, A. F. Panchula, and P. C. Canfield, Thermodynamics of spin  $s = 1/2$  antiferromagnetic uniform and alternating-exchange Heisenberg chains, *Phys. Rev. B* **61**, 9558 (2000).
- [61] V. Y. Krivnov, D. V. Dmitriev, S. Nishimoto, S.-L. Drechsler, and J. Richter, Delta chain with ferromagnetic and antiferromagnetic interactions at the critical point, *Phys. Rev. B* **90**, 014441 (2014).
- [62] D. C. Johnston, R. J. McQueeney, B. Lake, A. Honecker, M. E. Zhitomirsky, R. Nath, Y. Furukawa, V. P. Antropov, and Y. Singh, Magnetic exchange interactions in  $\text{BaMn}_2\text{As}_2$ : A case study of the  $J_1$ - $J_2$ - $J_c$  Heisenberg model, *Phys. Rev. B* **84**, 094445 (2011).
- [63] H.-J. Schmidt, A. Lohmann, and J. Richter, Eighth-order high-temperature expansion for general Heisenberg hamiltonians, *Phys. Rev. B* **84**, 104443 (2011).
- [64] A. Honecker, J. Schulenburg, and J. Richter, Magnetization plateaus in frustrated antiferromagnetic quantum spin models, *J. Phys.: Condens. Matter* **16**, S749 (2004).
- [65] H. Schlüter, J. Richter, and J. Schnack, Melting of magnetization plateaus for kagomé and square-kagomé lattice antiferromagnets, *J. Phys. Soc. Japan* **91**, 094711 (2022).
- [66] J. Schulenburg, A. Honecker, J. Schnack, J. Richter, and H.-J. Schmidt, Macroscopic magnetization jumps due to independent magnons in frustrated quantum spin lattices, *Phys. Rev. Lett.* **88**, 167207 (2002).
- [67] M. E. Zhitomirsky and H. Tsunetsugu, Exact low-temperature behavior of a kagomé antiferromagnet at high fields, *Phys. Rev. B* **70**, 100403 (2004).
- [68] O. Derzhko, J. Richter, A. Honecker, and H.-J. Schmidt, Universal properties of highly frustrated quantum magnets in strong magnetic fields, *Low Temp. Phys.* **33**, 745 (2007).
- [69] O. Derzhko and J. Richter, Universal low-temperature behavior of frustrated quantum antiferromagnets in the vicinity of the saturation field, *Eur. Phys. J. B* **52**, 23

- (2006).
- [70] T. Misawa, Y. Motoyama, and Y. Yamaji, Asymmetric melting of a one-third plateau in kagome quantum antiferromagnets, *Phys. Rev. B* **102**, 094419 (2020).
- [71] Y. Shirata, H. Tanaka, A. Matsuo, and K. Kindo, Experimental realization of a spin-1/2 triangular-lattice Heisenberg antiferromagnet, *Phys. Rev. Lett.* **108**, 057205 (2012).
- [72] Y. He, M. P. Zaletel, M. Oshikawa, and F. Pollmann, Signatures of Dirac cones in a DMRG study of the kagome Heisenberg model, *Phys. Rev. X* **7**, 031020 (2017).
- [73] X. Chen, S.-J. Ran, T. Liu, C. Peng, Y.-Z. Huang, and G. Su, Thermodynamics of spin-1/2 kagomé Heisenberg antiferromagnet: algebraic paramagnetic liquid and finite-temperature phase diagram, *Science Bulletin* **63**, 1545 (2018).
- [74] R. Schäfer, I. Hagymási, R. Moessner, and D. J. Luitz, Pyrochlore  $s = \frac{1}{2}$  Heisenberg antiferromagnet at finite temperature, *Phys. Rev. B* **102**, 054408 (2020).
- [75] P. Müller, A. Zander, and J. Richter, Thermodynamics of the kagome-lattice Heisenberg antiferromagnet with arbitrary spin  $s$ , *Phys. Rev. B* **98**, 024414 (2018).
- [76] R. Rausch, C. Plorin, and M. Peschke, The antiferromagnetic  $S = 1/2$  Heisenberg model on the  $C_{60}$  fullerene geometry, *SciPost Phys.* **10**, 87 (2021).
- [77] P. Schmoll, C. Balz, B. Lake, J. Eisert, and A. Kshetrimayum, Finite temperature tensor network algorithm for frustrated two-dimensional quantum materials (2022), [arXiv:2211.00121 \[cond-mat.str-el\]](https://arxiv.org/abs/2211.00121).